Hidden order in the frequency noise of an electronic oscillator

C. Eckert,[1] M. Planat,[2] and J. A. Miehé[1]
[1]*Groupe d'Optique Appliquée, Centre de Recherches Nucléaires, 23 rue du Læss, 67200 Strasbourg, France*
[2]*Laboratoire de Physique et Métrologie des Oscillateurs, 25044 Besançon Cedex, France*
(Received 19 June 1996)

The frequency noise of an electronic oscillator is investigated by measuring and analyzing the temporal fluctuations of its period. Two devices allow the recording of the variations of the average frequency of the oscillator and of its instantaneous time phase. In order to see if an underlying chaotic process can account for these fluctuations, the time series are analyzed with the help of three different methods. Two of them rely on the reconstruction of an embedding space, whereas the third is a multifractal-type approach. All the results lead to the same conclusion: the temporal fluctuations are consistent with the presence of a low-dimensional attractor that may be responsible for the remote correlations detected in the dynamical behavior. [S1063-651X(96)04812-X]

PACS number(s): 05.40.+j, 72.70.+m, 05.45.+b

I. INTRODUCTION

The low-frequency noise of an oscillator (quartz oscillator, atomic clock, etc.) is currently analyzed by the use of two basic tools: Allan variance and power spectral density [1]. Allan variance is defined as the mean-squared value $\sigma_y^2(\tau)=\frac{1}{2}\langle[\Delta y_i(\tau)]^2\rangle$ of the deviations $\Delta y_i(\tau)=y_{i+1}(\tau)-y_i(\tau)$ between successive frequency measurements, each sampled over a time interval τ. Typically, $\sigma_y^2(\tau)$ follows a power law τ^{-q} (q integer) over a restricted range of τ, with $q>0$ (convergence) over short times, $q=0$ (flicker noise floor) at intermediate times, and $q<0$ (divergence) at long times. The short-time dependence results from thermal noise ($q=2$) in quartz oscillators or masers and shot noise ($q=1$) in cesium clocks. However, the behavior observed at intermediate- and long-time scales is still unexplained.

The power spectral density is the second tool. It also follows a power law f^p (p integer) whose exponent is simply related to q by $q=p+1$ if $-3<p\leqslant 1$, and $q=2$ if $p\geqslant 1$ for stationary processes. In particular, shot noise in an atomic clock leads to white frequency noise ($p=0$), whereas the flicker floor ($q=0$) corresponds to a $1/f$ noise.

The ambiguity on the type of noise when $q=2$ is overcome by the modified Allan variance, which averages over N_s samples so that the effective bandwidth of the measurement decreases from $1/\tau$ to $1/N_s\tau$. However, there is no physical explanation for the origin of $1/f$ noise.

An alternative characterization of the stability [2] is based on a multifractal-type approach, which involves a three steps procedure. First, local scaling exponents are computed from the original data. The resulting series of exponents is then transformed into a binary coding, which gives valuable insights into the global stability of the system. The last step consists in constructing a ''devil's staircase'' from the coding to gain topological indications about the origin of the noise.

In addition, Lorentz [3] initiated the development of a variety of techniques to analyze erratic time series. Indeed he showed that the complexity may be only apparent, that is, the behavior is not necessarily stochastic but may result from a low-dimensional deterministic chaos. In order to distinguish between stochastic and deterministic processes, the analysis of time series generally begins by reconstructing an embedding phase space with the time delays method [4,5]. In the presence of deterministic chaos, the attractor of the system is thus unfolded, so that its dynamical properties can be extracted. The correlation dimension [6], the Kol'mogorov entropy [7], the phase portraits and Poincaré sections [8], and the Lyapunov exponents [9] are some features that can be estimated. In practice, the presence of an attractor is presupposed and the ability to detect invariants is taken as a proof of its existence. Unfortunately, it has been shown [10–12] that this approach can be misleading. Some stochastic processes give rise to a seeming invariant and, conversely, the determination of the invariants of a chaotic system may be hindered by the experimental noise. These drawbacks have motived the emergence of new methods [13,14] that are not based on the calculation of some dynamical properties, but instead rely on the topology of the points in the reconstructed phase space to check the presence of an embedded attractor.

The purpose of this paper is to investigate temporal fluctuations of electronic oscillators with the aim to detect a possible low-dimensional deterministic process. The two kinds of experiments used to measure these fluctuations are briefly described in Sec. II. The time series analyzes based on the reconstruction of an embedding space are carried out in the succeeding section by estimating the correlation dimension (Sec. III A) and by investigating the topological properties of the reconstructed space (Sec. III B). The multifractal-type approach is implemented in Sec. IV. The significant results are finally summarized, and the work is concluded by a short discussion in relation to nonlinear dynamical systems represented by the Arnol'd map.

II. EXPERIMENTAL ARRANGEMENTS

The stability of oscillators can be studied in time or frequency domains. In the present paper, two kinds of time domain experiments are considered. In one case (Sec. II A) one measures fluctuations of the average frequency, whereas the other (Sec. II B) leads to the recording of instantaneous

phase fluctuations. Two characteristic times have been proved [15] to have a major influence on the variations of the measured quantity (frequency or phase) y. These are the sampling duration τ, that is, the time interval during which y is accumulated, and the sampling period Δt, which represents the time elapsed between the beginning of two consecutive recordings of y. The difference $\Delta t-\tau$ is the so-called dead time. Thus the outcomes are a collection of $y_i(\tau,\Delta t)$, where y_i stands for the ith measurement of y. In this regard, the two experiments are complementary. Indeed, the average frequency is continuously monitored, that is to say the dead time is equal to zero and $\Delta t=\tau$, whereas the phase measurement is instantaneous ($\tau=0$), so that the dead time is equal to the sampling period Δt.

A. Period counting technique

Period counting is the common technique of average frequency measurements with a counter. The oscillator signal being tested is mixed to a reference signal of nearly the same frequency to produce a low-frequency beat signal. This signal is introduced as a trigger to a gate in the reciprocal counter, which opens at one of its zero crossing. The high-frequency counter clock signal and the beat signal are accumulated in the counter register and their periods are simultaneously counted. The gate closes after an integral number of cycles of the counter oscillator, which determines the sampling duration τ. In this way the resolution τ_0/τ only depends on the period τ_0 of the 500-MHz counter clock and on the sampling duration τ. In most of the reported recordings the resolution was made equal to 2×10^{-9} by sampling during 1 s. After each sampling, the number of cycles of the beat at 101 Hz of two 2.56-MHz oscillators is divided by τ to yield the average frequency. The beat is continuously sampled so that two consecutive measurements are adjacent (no dead time) and one can use the shortened notation $y_i\equiv y_i(\tau,\tau)$, where $\tau=1$ s unless otherwise specified.

B. Instantaneous time phase measurement

In this experiment, individual laser pulses are recorded by a synchroscan streak camera associated with an optical multichannel analyzer and a microcomputer. The sweep of the camera is generated by frequency doubling the signal of the electronic oscillator, which drives the mode locker of the laser. It has been shown [16,17] that the barycenter of the streak image is directly related to the time interval between the arrival time of the pulse and the instant of zero crossing of the sweep, so that the sampling duration τ is equal to zero. Moreover, a comparison between experimental results and those deduced from a model evidences [17] that the laser jitter is less than 3 ps. Therefore, the temporal behavior of the barycenters (Fig. 1) reflects the instantaneous time phase fluctuations ($\sim$20 ps) of the mode locker oscillator. Experimentally, the train of picosecond pulses is delivered by a dye laser pumped by a Nd:YAG laser (where YAG denotes yttrium aluminum garnet) which is mode locked by an acousto-optic modulator driven at 40 MHz. The deflection of the camera is equal to 0.93ps/channel. Each recording consists in 1024 measurements spaced by a sampling period $\Delta t=40$ ms. This is all that is needed to define

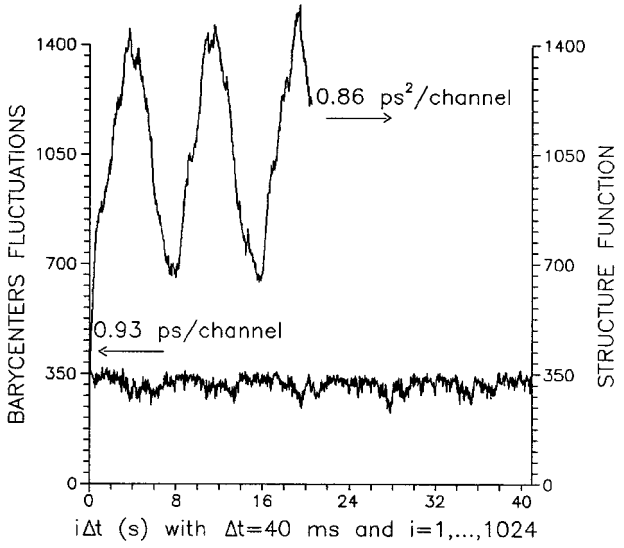

FIG. 1. Temporal fluctuations and structure function [18] of the pulse positions recorded with the streak camera.

$y_i\equiv y_i(0,0.04)$ as the ith measurement, but more details about the experimental arrangement can be found in [16,17].

III. EMBEDDED TIME SERIES ANALYSIS

The time delay method [4] amounts to construct a collection $\{\vec{Y}_i, i=0,N_v-1\}$ of m-dimensional vectors

$$\vec{Y}_i=(y_{ik},y_{ik+l},y_{ik+2l},\ldots,y_{ik+(m-1)l}) \tag{1}$$

from the scalar time series $\{y_i, i=0,N_p-1\}$ for given delays k,l and embedding dimension m. The embedding theorem [5] states that, in the case of a system whose trajectory lies on a d-dimensional attractor, the space underlying the dynamics of the system can be unfolded by a proper choice (K,L,M) of the parameters (k,l,m).

The delays k and l are intended to rule out dynamically close points, that is, points for which $y_{i+1}\sim y_i$ due to a small sampling period Δt. Different methods [19] have been suggested to determine the delay l between successive coordinates of a vector. The delay k between the first components of successive vectors was introduced by Albano *et al.* [20] and can be used to settle the anomaly mentioned by Theiler [21]. The embedding dimension m must be chosen sufficiently large for the embedding space to unfold the geometry of the attractor. This condition is surely met [5] if $m>2d$, but the minimal sufficient embedding dimension M may be smaller.

The time delay procedure is the starting point of the various techniques proposed to detect a possible attractor in a time series. Two of them are considered, one consisting in the estimation of the correlation dimension and the other based on topological considerations.

A. Correlation dimension

The Grassberger-Procaccia algorithm [6] amounts to calculating the correlation integrals

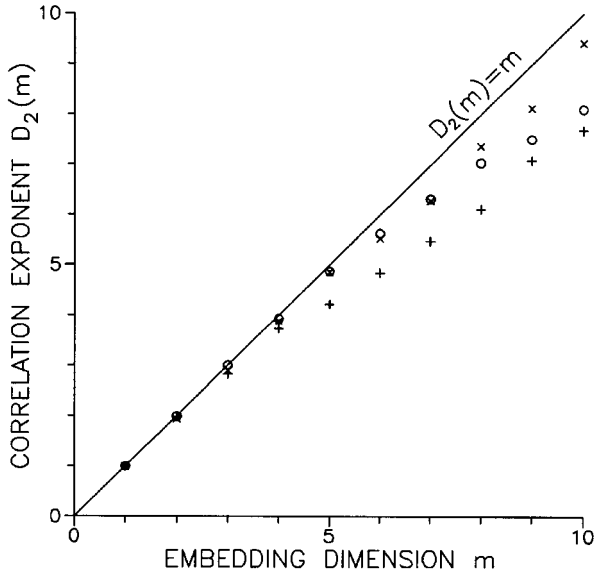

FIG. 2. Correlation exponents of a beat frequency recording (○) and experimental (+) and simulated (×) phase fluctuations. The embedding delays are $k=l=1$. The straight line of slope 1 is also shown.

$$C(m,r)=\frac{2}{N_v(N_v-1)}\sum_{i=0}^{N_v-2}\sum_{j=i+1}^{N_v-1}H(r-|\vec{Y}_i-\vec{Y}_j|) \quad (2)$$

for increasing embedding dimensions m. Here $H(r)$ is the Heaviside function and $|\vec{Y}_i-\vec{Y}_j|$ is the Euclidian distance between $\vec{Y}_i$ and $\vec{Y}_j$ (excluding $\vec{Y}_i$ itself), so that $\Sigma_j H(r-|\vec{Y}_i-\vec{Y}_j|)$ counts the number of vectors $\vec{Y}_j$ that lie in the m-dimensional ball of radius r centered at $\vec{Y}_i$. The number N_v of constructed vectors is related to the number N_p of points in the original data set by $N_v=1+[N_p-1-(m-1)l]/k$. Thus $C(m,r)$ is the fraction of pairs of embedded vectors closer than r. In the presence of a strange attractor, it has been shown [6] that at small r the correlation integral displays a scaling region

$$\lim_{N_v\to\infty,\,r\to 0} C(m,r)=r^{D_2(m)} \quad (3a)$$

whose exponent $D_2(m)$ becomes constant at sufficiently large m. The resulting correlation dimension

$$D_2=\lim_{m\to M} D_2(m) \quad (3b)$$

is a lower bound of the fractal dimension [6].

The correlation integrals have been computed according to Eq. (2) for several time series obtained from the experiments described in Sec. II. The data were successively embedded in dimensions 1–10 using the same value for both delays: $k=l=1$. The length scale has been normalized such that the diameter of the embedding space is equal to one. In all cases, double logarithmic plots of $C(m,r)$ versus r showed a scaling behavior in the range of small r from which $D_2(m)$ is determined. The exponents are represented versus m in Fig. 2 for one time series recorded with each experimental device. Also shown in this figure are the results arising from a time series computed with the help of a model [17], developed to interpret the pulse fluctuations recorded with streak cameras, by assuming that the laser and electronic oscillators undergo white Gaussian fluctuations. As can be seen on the figure, no significant difference is observed between the various cases, except that the correlation exponents resulting from the simulated data are closer to the straight line than the others. There is no saturation of the slope with increasing m, so that D_2 cannot be determined.

In their paper [6], Grassberger and Procaccia suggested that their method allows one to distinguish between a chaotic and a stochastic process for in the latter case the correlation integrals are expected to scale like r^m. However, Fig. 2 shows that, as they present no clear saturation, the correlation exponents $D_2(m)$ do not follow the straight line $D_2(m)=m$.

The results obtained from the above analysis are quite elusive, for neither of the expected behaviors are observed. Even the correlation exponents of the simulated time series, which is known to depict a white noise, do not follow the straight line as they should. Nevertheless, they are greater than the $D_2(m)$ of the experimental data, and the difference increases with m so that the experimental and simulated time series cannot be considered as behaving alike. Several ways of improving the algorithm have been proposed [10,20–22], but it has been verified [23] that the correlation exponents presented in Fig. 2 are not sensitive to these modifications nor to the variation of the delays k and l. This robustness is not surprising because the problem with the integral correlation method is that short-time correlations can greatly affect the outcomes. However, this drawback is not effective in the present work since the recording of the instantaneous phase (mean frequency) is performed with a sampling period (sampling duration) that is long compared to typical time scales of their fluctuations.

The failure of the method has to be sought in the experimental limitations. Indeed, neither of the limits involved in Eq. (3a) can be reached. On the one hand, an increase in N_v increases the recording and computing times. On the other hand, the limit $r\to 0$ is prevented because of the precision of the measurements and the experimental noise. The latter is at least equal to the error introduced by rounding off the data and leads to an overestimation of $D_2(m)$. Moreover, the incertitudes increase with m since the density of points in the embedding space lowers, whereas the contribution of the noise grows. In this regard, there have been a number of attempts [24–26] to connect the maximum correlation dimension attainable to the length N_p of the time series. These relations yield a lower (pessimistic) bound of about 2 and an upper (optimistic) bound of the order of 5 for the lengths of the considered data. Thus, the correlation exponents reported in Fig. 2 can result from a stochastic process or from a chaotic system, of dimension greater than 2, blurred by the experimental noise. It is therefore of importance to dispose of another method that works for short-time series and is less sensitive to the noise.

B. False neighbor methods

As an introduction, it is worth recalling that the method presented in the preceding subsection amounts to computing

some invariant of the attractor, namely, its correlation dimension. Nevertheless, when applied to actual data, the method is in fact used to check the existence of the attractor: if a finite value of D_2 can be found, it is inferred that the attractor does exist. The false-neighbor methods are thoroughly different, for, rather than presupposing the attractor's existence, they make use of topological arguments to see if the attractor really exists.

1. Description

The false-neighbor methods [13,14] use geometrical considerations to compare the vectors constructed in m- and $(m+1)$-dimensional spaces. This enables one to identify false neighbors, that is, points that appear to be neighbors because the embedding dimension is too small. To illustrate this, consider a system for which the appropriate embedding dimension is $M=2$ and the attractor is a circle, for example. If embedded in a one-dimensional space, all the points of the attractor lie on a straight line, but points that are close on this line may come from opposite quarters of the circle. Hence they are false neighbors. Conversely, for $m \geqslant 2$, the circle remains unaltered and all the neighbors are true neighbors. Thus the preservation of neighborhood relations can be taken as a criterion for the determination of the minimal acceptable embedding dimension.

Given a reference point $\vec{Y}_i$ of the m-dimensional embedding space, let $\vec{Y}_{i,n(m)}$ be its nth nearest neighbor. In going from dimension m to $m+1$, $\vec{Y}_i$ gets a $(m+1)$th coordinate, namely, $\vec{Y}_{ik+ml}$, and its nth nearest neighbor now is $\vec{Y}_{i,n(m+1)}$. In the Euclidian metric, the squared distances between $\vec{Y}_i$ and its n^{th} nearest neighbor are

$$D_m(i,n(m)) \equiv |\vec{Y}_{i,n(m)} - \vec{Y}_i|^2 \tag{4a}$$

and

$$D_{m+1}(i,n(m+1)) \equiv |\vec{Y}_{i,n(m+1)} - \vec{Y}_i|^2 \tag{4b}$$

in m and $m+1$ dimensions, respectively.

The averaged wavering product [13] is defined by

$$\overline{W} = \ln \left\langle \prod_{n=1}^{w} \left[\frac{D_m(i,n(m))}{D_m(i,n(m+1))} \frac{D_{m+1}(i,n(m))}{D_{m+1}(i,n(m+1))} \right]^{1/w} \right\rangle_i . \tag{5}$$

Both ratios compare the distance between $\vec{Y}_i$ and $\vec{Y}_{i,n(m)}$ with the distance between $\vec{Y}_i$ and $\vec{Y}_{i,n(m+1)}$, yet they are computed in m and $m+1$ dimensions for the first and second ratios, respectively. If the nth nearest neighbor in m dimensions remains the nth nearest neighbor in $m+1$ dimensions, the two quotients are equal to one. So, if the topological properties of the supposititious attractor are retrieved in m dimensions, $\overline{W}$ should be equal to zero. In fact, because of the addition of a new coordinate in going from m to $m+1$, the order of the neighbors may slightly vary even if the repartition of the points is unchanged on the whole, that is, even if an attractor is embedded in the m-dimensional space. The effect of this ordering variation, which is to unjustly keep off the two ratios appearing in Eq. (5) from 1, is prevented by the geometric mean from $n=1$ to $n=w$. The wavering product is arithmetically averaged over several reference points $\vec{Y}_i$ in order to restitute the behavior of all the embedding space. Small deviations from one are enlarged by considering the logarithm. Thus $\overline{W}$ approaches 0 when the number of false neighbors diminishes.

The averaged wavering product depends not only on m, but also on the lags k and l. When $\overline{W}$ is plotted as a function of l for various m, the appropriate lag L and embedding dimension M are determined as those for which $\overline{W}$ is minimal as a function of l and does not significantly decrease further if the dimension increases. The variation of the third parameter k likewise enables one to settle its proper value K. It must be pointed out that it is not the behavior of $\overline{W}/l\Delta t$, as suggested in [13], that is analyzed, but the behavior of $\overline{W}$. Indeed, dividing the dimensionless quantity $\overline{W}$ by $l\Delta t$ would make the result dependent on the experimental time scale, which is not necessarily related to the characteristic time scale of the examined process. In particular, increasing Δt would arbitrarily decrease the averaged wavering product. This agrees with the comments of Kennel, Brown, and Abarbanel [14] and of Liebert, Pawelzik, and Schuster [13], who noted that greater l ''only seem to be similarly appropriate, due to our rescaling of the wavering product.''

Another way to study the topological properties of the phase space is to compute the false-nearest-neighbors percentage [14]. It amounts to comparing the m- and $(m+1)$-dimensional distances between $\vec{Y}_i$ and its first neighbor $\vec{Y}_{i,1(m)}$ in m-dimensional space. For a given tolerated relative increase of the distance R_{tol}, if

$$\frac{D_{m+1}(i,1(m)) - D_m(i,1(m))}{D_m(i,1(m))} > R_{\text{tol}}^2 \tag{6a}$$

is verified, then $\vec{Y}_{i,1(m)}$ is considered as a false neighbor. As noted by Kennel, Brown, and Abarbanel, this criterion is not sufficient for actual data because of their limited length. Indeed, even for white noises, the number of false neighbors identified by (6a) may decrease when m increases, for $\vec{Y}_{i,1(m)}$ may be the first neighbor of $\vec{Y}_i$ even it is not close to it. This results in an already large value of $D_m(i,1(m))$, so that the relative increase may be small. To prevent this, a second criterion has been introduced [14]: if

$$D_{m+1}(i,1(m)) > F_{\text{tol}} \sigma^2(y), \tag{6b}$$

where F_{tol} is some tolerance factor and $\sigma^2(y)$ is the variance of the data, the neighbor is declared as false. The false-nearest-neighbor percentage is computed by applying both criteria: for a given reference point, its first neighbor is declared as false if either Eq. (6a) or (6b) is satisfied. All the embedded vectors are tested to count the number of false neighbors. This number is finally divided by N_v to get a quantity, namely, the percentage, independent of the length of the time series.

In this method, a too small embedding dimension results in a high value of the false-nearest-neighbor percentage because many neighbors are removed in passing from m to $m+1$. Conversely, when m is sufficiently large to unfold the

attractor, the number of false neighbors drops to zero. The alterations of the false-nearest-neighbor percentage induced by the variation of k and l allow one to fix their proper values K and L. Thus both of the false-neighbor methods provide a way to check the presence of an attractor and to assess the embedding dimension and lags. Moreover, compared to the methods fated to the estimation of attractor invariants, their requirements in terms of time series length, experimental noise, and computing time are less stringent.

2. Application

Each false-neighbor method has been implemented on several time series. Although it has been suggested [13] to perform the geometrical average in Eq. (5) over ten neighbors (if $N_v = 10\,000$) and the arithmetic mean over about 10% of the data, the influence of both w and the number of reference points considered has, nevertheless, been examined. It is found that W slightly changes when w is varied, but the general trends of the dependence of W on k, l, and m are unaffected. The number of reference points considered influences both the value of W and its dependence on the embedding parameters. This is probably due to the shortness of the time series ($N_p = 1024$, 2500, or 5000), so the arithmetic mean was performed over all the N_v embedded points. Whatever the considered time series, the averaged wavering product computed according to Eq. (5) is quite indifferent to the values of the lags k and l. The same behavior was observed for the correlation exponents and is likewise explained (see Sec. III A). Concerning the effect of m, it appears that W diminishes by a factor of 10 when the embedding dimension increases from $m = 1$ to $m = 10$. Unfortunately, the determination of a proper embedding dimension is intricate because no convergence of W is observed: when m is incremented W decreases, though less and less, without reaching zero. This may be due [14] to the inherent experimental noise. However, the estimation of M would require one to have an idea of the value of W that can be considered as negligible or is reached when all the neighbors are false neighbors.

For the calculation of false-nearest-neighbor percentages, the tolerance factor was fixed at $F_{\mathrm{tol}} = 4.0$ [14]. The allowed relative distance increase R_{tol} was kept as a parameter in order to appreciate its influence. The effect of varying the lags was investigated, but, as previously, no significant modification was detected, so it can safely be inferred that $K = L = 1$. The results of jointly applying the criteria given by Eqs. (6) for various R_{tol} are shown for an experimental [Fig. 3(a)] and a simulated [Fig. 3(b)] time series of instantaneous time phase. In both cases, the false-nearest-neighbor percentage sharply decreases when the embedding dimension is incremented from $m = 1$ to $m = 3-5$, depending on R_{tol}. Considering the experimental time series, for example, 6.8%, 5.4%, and 4.8% of the false neighbors are left for $R_{\mathrm{tol}} = 5$, 10, and 15, respectively. Other features are common to both drawings: when m is further incremented the percentage of false neighbors increases and the sensitiveness on R_{tol} vanishes when $m \geqslant 6$. A similar behavior is observed for the beat measurements. Figure 4 shows the results for R_{tol} fixed but different sampling durations. It is seen that the false-nearest-neighbor percentage diminishes when the beats

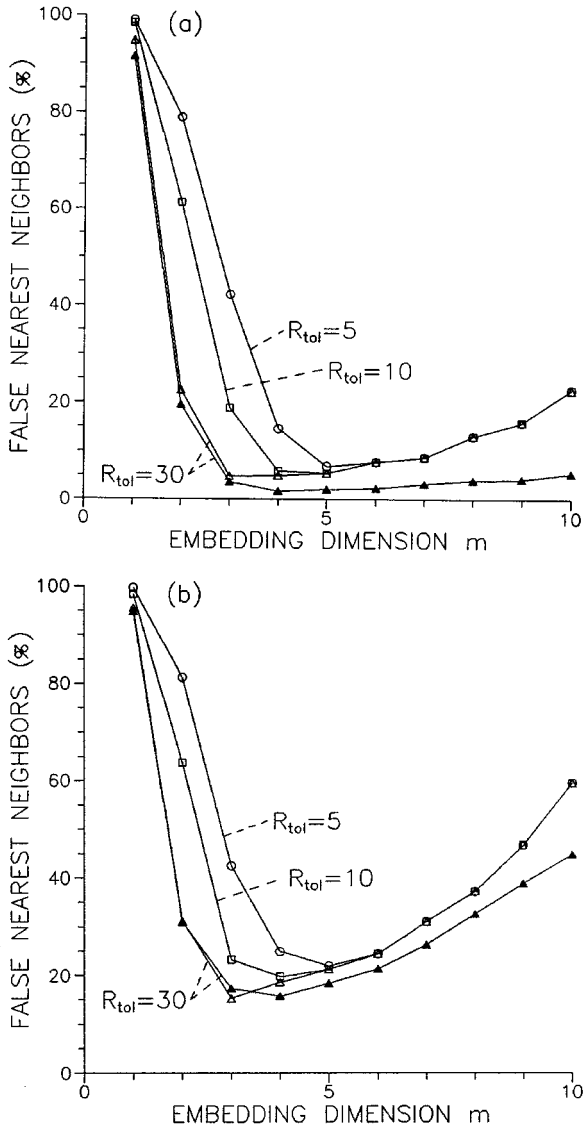

FIG. 3. False-nearest-neighbor percentage of (a) experimental and (b) simulated phase fluctuations, before (empty symbols) and after (filled symbols) noise reduction. The embedding delays are $k = l = 1$.

are longer averaged and the convergence is improved. For sampling durations greater than 1 s, the increase of the curves beyond their minimum is almost invisible.

As far as the recognition of an underlying attractor is concerned, the embedding dimension for which the false-nearest-neighbor percentage is minimal has to be determined. This involves the estimation of the proper R_{tol}. It should not be chosen too small, because the embedding procedure always leads to an increase of the distances, but it should neither be chosen too high, so that none of the false neighbors is missed. It has been suggested [14] to take $R_{\mathrm{tol}} \sim 10-15$. As can be seen from Fig. 3, the decrease of the false-nearest-neighbor percentage is specially manifest for low values of m and R_{tol} increasing to $15-20$. However, in some cases the minimum of the false-nearest-neighbor percentage goes to a lower value of m when R_{tol} is further increased. The independence on R_{tol} observed for larger embedding dimensions results from the limited number of data.

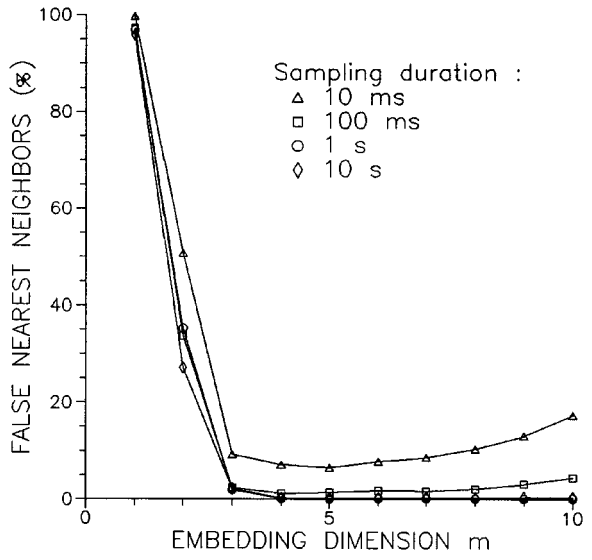

FIG. 4. False-nearest-neighbor percentage of beat frequency data measured with various sampling durations τ. The embedding delays are $k=l=1$. $R_{\mathrm{tol}}=30$.

Indeed, the density of points in the phase space lowers, so that the distance between $\vec{Y}_i$ and its nearest neighbor is large and $\vec{Y}_{i,1(m)}$ is considered as a false neighbor owing to the second criterion (6b). This interpretation is corroborated by considering that the false-nearest-neighbor percentage becomes independent of R_{tol} for $m \geqslant 6$ (Fig. 3), 7, and 8 when $N_p=1024$, 2500, and 5000, respectively. On the whole, it seems that $R_{\mathrm{tol}}=10-30$ is suited for the analysis of the dependence of the false-nearest-neighbor percentage on m and consequently for the estimation of the minimal acceptable embedding dimension.

3. Effect of experimental noise

Taking into account that actual time series always are noisy, it remains to ascertain if the residual false neighbors can be viewed as an effect of the noise, in which case the presence of an attractor can be inferred, or if this residue is the manifestation of a stochastic process. In this regard it must be noted that the false-nearest-neighbor percentage is more informative than the averaged wavering product because it is bounded between 0 and 100, so that the percentages of different time series can easily be compared. In particular, the residual false-nearest-neighbor percentage of the simulated time series [Fig. 3(b)] is three to four times greater than that of the experimental recordings [Fig. 3(a)]. Such a difference is not observed for the averaged wavering product. Remembering that the simulated data have been computed for white noises [17], the results shown in Figs. 3 suggest that the experimental time series might be the superposition of a deterministic process and a noise. Since the measurements performed with the streak camera contain both the instantaneous time phase fluctuations of the electronic oscillator and the smaller laser jitter [17], the $\sim 5\%$ residual false-nearest-neighbor percentage may itself arise from the superposition of the true experimental noise and a stochastic process. The implication of the noise is still more obvious for the mean frequency measurements (Fig. 4). Indeed, the residual percentage amounts to 6.6 % and 1.2% for a sampling duration of 10 and 100 ms, respectively, and drops almost to 0 when the beats are longer averaged. This decrease of the residue can be understood as an effect of the smoothing of the noise during a longer time interval.

The presence of an underlying attractor has been further checked by implementing two additional tests. The first consists of taking advantage of the false-nearest-neighbor percentage to determine a starting embedding dimension m_0, applying a method of noise reduction [27] in the m_0-dimensional embedding space, and computing the false-nearest-neighbor percentage of the cleaner time series. This test was applied for $m_0=6$ to data recorded with the streak camera and to simulated time series. The outcomes are shown in Fig. 3, for $R_{\mathrm{tol}}=30$, together with the results obtained from the original time series. The false-nearest-neighbor percentage is minimal for $m=4$ for both experimental and computed data. However, in the latter case the effect of the noise reduction is weak, whereas the residue drops to 1.7% for the experimental data. The difference between the two time series also reflects on the behavior for $m \geqslant 5$: for the simulated fluctuations [Fig. 3(b)] the curves corresponding to the original and cleaned data are nearly parallel, whereas the false-nearest-neighbor percentage of the cleaned experimental time series [Fig. 3(a)] presents a plateau. Thus the noise reduction supports the preceding conclusions: the simulated time series has a behavior characteristic of a stochastic process, whereas the experimental time phase fluctuations of the oscillator are consistent with an underlying attractor.

The second test follows from an objection [28] to the ability of the false-nearest-neighbor percentage to distinguish between stochastic and deterministic processes. The idea is that neighbors considered as true neighbors according to the criteria of Eqs. (6) may be neighbors in space only because they are neighbors in time and not, as they should, because they are in a region that has been visited several times during the recording of the data. This shortcoming is the same as that mentioned in Sec. III A, and indeed the proposed remedies [28] are similar. However, for all the time series considered, the mean time separation between the reference points and their nearest neighbor is always greater than 300 (in sampling units), and exceeds 1300 for some of the time series handled in Fig. 4. Since these values are large compared to the number of available data and, most important, nearly independent of the embedding dimension, the same prior conclusion intrudes: the analysis is not warped by short-time correlations of the time series studied.

Thus these verifications do not weaken the conclusions drawn from the naive application of the false-nearest-neighbor percentage method. The time series obtained by recording either the instantaneous time phase or the beats of an oscillator are in agreement with a dynamical process in which a noise is superimposed to a deterministic system with few degrees of freedom. The underlying attractor might be unfolded in an embedding phase space of dimension as small as $M=4-6$. The independence of the results on the lags involved in the reconstruction procedure is due to the large sampling period or duration, but might no more be accurate if the instantaneous time phase is recorded at a higher repetition rate or if the beats are averaged over a shorter time.

IV. MULTIFRACTAL-TYPE APPROACH

A. Local convergence analysis

An alternative characterization of the frequency noise of an oscillator has been developed [2] in the spirit of convergence analysis of series. From the original time series $\{y_i, i=0, \ldots, N_p-1\}$ several sets of deviations $\{\Delta^{(N_s)}y_i, i=0,1, \ldots, N_p-N_s-1\}$, where

$$\Delta^{(N_s)}y_i=\frac{1}{N_s}\left[\sum_{j=i+N_s}^{i+2N_s-1} y_j-\sum_{j=i}^{i+N_s-1} y_j\right], \tag{7}$$

are constructed by averaging over N_s samples.

From Eq. (7) it is seen that if no average is performed ($N_s=1$), $\Delta^{(1)}y_i$ is merely one of the terms involved in the Allan variance. For $N_s\neq 1$, $\Delta^{(1)}y_i$ can be viewed as the deviation that would result if the sampling duration were $N_s\tau$. However, $\Delta^{(N_s)}y_i$ and $\Delta^{(N_s)}y_{i+1}$ only differ because of the two extreme and the two middle terms, so that $N_s\tau$ can be considered as a sliding window, whereas for a sampling duration of $N_s\tau$ the next accessible deviation after $\Delta^{(N_s)}y_i$ would be $\Delta^{(N_s)}y_{i+N_s}$.

By comparing $\Delta^{(N_s)}y_i$ to the general term of a Riemann series $\Sigma_{\tau=0}{}^{\infty}\tau^{-\beta}$ and bearing in mind that absolute convergence implies convergence, a local scaling exponent

$$\beta_i^{(N_s)}=-\frac{\ln|\Delta^{(N_s)}y_i|}{\ln(N_s\tau)} \tag{8}$$

is defined. It can be noted that this terminology agrees with the intuitive approach of oscillators stability: small fluctuations of the experimental data lead to low values of $\Delta^{(N_s)}y_i$, whence a high scaling exponent, and indeed the Riemann series converges if and only if $\beta>1$.

The deviations $\Delta^{(N_s)}y_i$ and scaling exponents $\beta_i^{(N_s)}$ have been computed from Eqs. (7) and (8) for several time series of instantaneous phase and average frequency. The results obtained with $N_s=25$ for instantaneous phase fluctuations are shown in Fig. 5(a). As expected, the highest exponents arise from the lowest phase deviations. If the data are not averaged ($N_s=1$), the local scaling exponents are sprayed over a wide range of values [Fig. 5(b)], but $\beta_i^{(N_s)}>1$ for the whole times series, which corresponds to the general term of a convergent Riemann series. When the sliding window increases the scaling exponents are smoothed, most of the $\beta_i^{(N_s)}$ decrease, and the remaining high exponents appear more and more as bursts (Fig. 5). The smooth part of the curve thus becomes characteristic of a divergent series ($\beta_i^{(N_s)}\leqslant 1$) and only the bursts indicate a convergence.

Being a matter of convergence or divergence, the experimental time series are too irregular to yield a limiting scaling exponent in the classical meaning of limits. The sets of $\beta_i^{(N_s)}$ therefore cannot be compared directly to the general term of a Riemann series. However, local discontinuities of the scaling exponents can be detected by performing a binary coding of the series. This is done by computing the quantities

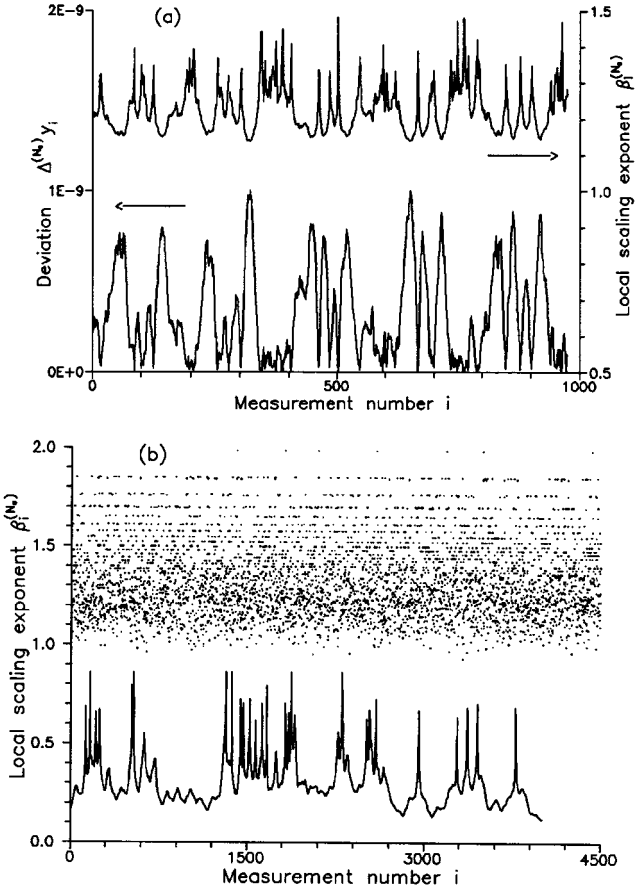

FIG. 5. (a) Deviations and local scaling exponents of experimental time phase data averaged over $N_s=25$. (b) Local scaling exponents of crude (upper curve) and averaged over $N_s=250$ (lower curve) beat frequency variations. For the sake of clarity, the lower curve has been decreased by 0.3.

$$\delta_i^{(N_s)}=1-\frac{\beta_{i+1}^{(N_s)}}{\beta_i^{(N_s)}}, \tag{9a}$$

which, according to Eq. (8), are connected to adjacent deviations by the relation

$$\frac{\Delta^{(N_s)}y_{i+1}}{\Delta^{(N_s)}y_i}=(N_s\tau)^{\beta_i^{(N_s)}\delta_i^{(N_s)}}. \tag{9b}$$

The resulting set of real numbers $\{\delta_i^{(N_s)}\}$ can be converted into a sequence of 0 and 1 by labeling small real numbers ($|\delta_i^{(N_s)}|<10^{-3}$) as 0 and the others as 1. The study of the initial time series is thus turned into that of a binary coding. From Eq. (9a) it can be inferred that the terms coded as 0 arise from nearly equal adjacent scaling exponents. This observation is to be compared with the features of the sets $\{\beta_i^{(N_s)}\}$ (Fig. 5). As noted before, the smooth parts of the curves correspond to low scaling exponents, which are themselves characteristic of an unstable behavior of the time series. The zones of the binary coding where $\delta_i^{(N_s)}=0$ can therefore be considered as an unstable set, whereas local stability leads to $\delta_i^{(N_s)}=1$.

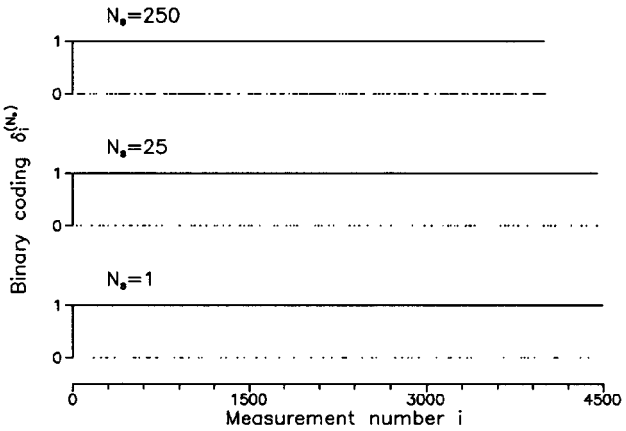

FIG. 6. Binary coding of beat frequency fluctuations averaged over different values of N_s.

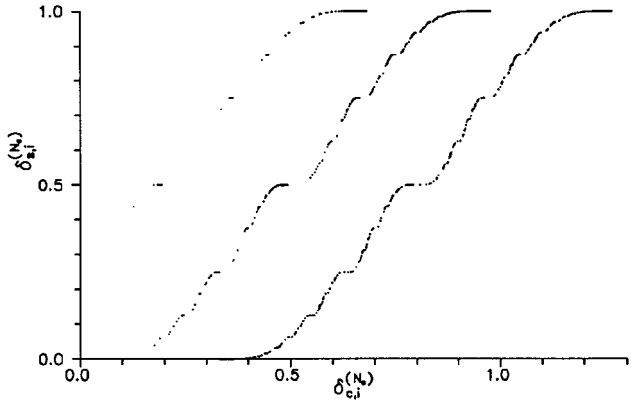

FIG. 7. Devil's staircase of experimental time phase fluctuations averaged over $N_s=1$,25, and 250 from left to right, respectively. For the sake of clarity, $\delta_{c,i}^{(N_s)}$ has been decreased (increased) by 0.3 for $N_s=1$ (250).

The sequences resulting from the binary coding of beat frequency fluctuations are reported in Fig. 6 for several sliding windows. As expected from the corresponding sets of local scaling exponents, the unstable clusters enlarge and become more numerous as N_s is increased. This is to be related to the smoothing of the curves $\{\beta_i^{(N_s)}\}$ for growing sliding windows. However, the binary coding enables a fine examination of the local stability. It is indeed observed that the unstable set, which reflects large fluctuations in the measured time series, is never empty, even when $\beta_i^{(N_s)}>1$ for the whole series (for example, if $N_s=1$). Thus the binary coding, to which four consecutive y_i contribute, emphasizes local instabilities that are hidden in the scaling exponent analysis where only two consecutive data are involved.

B. Global convergence analysis

The last step in the multifractal-type approach is the study of the global convergence. Here the binary sequence is analyzed as a whole. To this end, two additional real numbers are defined:

$$\delta_{s,i}^{(N_s)}=\frac{1}{2}\sum_{j=0}^{\infty}\delta_{i+j}^{(N_s)}2^{-j}, \tag{10a}$$

$$\delta_{c,i}^{(N_s)}=n_{0i}+1/\{n_{1i}+1/[n_{2i}+1/(n_{3i}+\cdots)]\}, \tag{10b}$$

where $n_{0i}=0\ \forall i$ and the other integers mean that the part of the binary coding that starts at $\delta_i^{(N_s)}$ is a sequence of $n_{1i}-1$ consecutive 0, followed by n_{2i} consecutive 1, n_{3i} consecutive 0, and so on. From their definition, the numbers calculated using Eqs. (10) lie in the interval [0,1]. For a structurally stable (or globally convergent) sequence, where there is a majority of bits of the same kind (0 or 1), the occurrence of a bit of alternative type (1 or 0) only weakly affects $\delta_{s,i}^{(N_s)}$ and $\delta_{c,i}^{(N_s)}$. In this case they rapidly converge to rational numbers: for $\delta_{c,i}^{(N_s)}$ it follows from the big integers entering into Eq. (10b), while for $\delta_{s,i}^{(N_s)}$ it is due to the presence (absence) of only few terms in Eq. (10a). Contrarily, a sequence with a discontinuous distribution of 0 and 1 is strongly sensitive to this distribution and indicates a structurally unstability (or ergodicity). The slippery devil's staircase [29], which represents $\delta_{s,i}^{(N_s)}$ as a function of $\delta_{c,i}^{(N_s)}$ is a monotonically increasing curve whose steps correspond to rational values of $\delta_{s,i}^{(N_s)}$ and $\delta_{c,i}^{(N_s)}$ The global convergence can be studied from the properties of this graph. For an uncorrelated binary sequence there are gaps at the steps locations [2] because the bits 0 and 1 are randomly distributed. On the contrary, a structurally stable sequence presents long ranges of identical bits, so that $\delta_{s,i}^{(N_s)}$ and $\delta_{c,i}^{(N_s)}$ are close to rational numbers and the staircase steps fill.

The devil's staircase built according to Eqs. (10) for a time series of instantaneous time phase measurements is reported in Fig. 7 for various sliding windows. From a practical point of view, it was found that the infinite summations of Eqs. (10) are well approximated with only 50 bits. If the data are not averaged ($N_s=1$), the staircase is almost reduced to the step corresponding to $\delta_{s,i}^{(N_s)}=\delta_{c,i}^{(N_s)}=1$, in agreement with the binary coding. Indeed, nearly all the bits belong to the stable set, so that Eq. (10a) appears as a geometrical progression whose limit is 1 when enough terms are involved, while Eq. (10b) is to be calculated for $n_{1i}=1$ and a high value of n_{2i} leading to $\delta_{c,i}^{(N_s)}\sim 1$ for almost every i. The occurrence of some bits 0 in the coding results in the filling of a few other steps, especially those attached to $\delta_{s,i}^{(N_s)}=\frac{1}{2},\frac{3}{4},\frac{7}{8}$. In particular, Eqs. (10) show that the filling of the step $\delta_{s,i}^{(N_s)}=\delta_{c,i}^{(N_s)}=1/2$ comes from the pieces of sequence whose first bit is $\delta_i^{(N_s)}=0$. In the same way that the increase of the sliding window transfers more and more bits to the unstable set of the coding, it leads to the filling of steps belonging to the lower part of the staircase and of steep parts of the curve located between steps.

The results of the multifractal-type approach can now be summarized. Applying Eq. (8) to a time series with small fluctuations results in high (>1) scaling exponents, indicating a local stability. However, for small deviations the exponent is very sensitive to $\Delta^{(N_s)}y_i$, so that the collection $\{\beta_i^{(N_s)}\}$ is highly discontinuous. Remembering that any $\delta_i^{(N_s)}\geqslant 10^{-3}$ is coded as 1, such collections $\{\beta_i^{(N_s)}\}$ nevertheless lead to a binary sequence mostly constituted of bits

equal to 1 that form a locally stable set, whereas the unstable set is sparse. Besides, the presence of long strings of bits of the same type (1 in this case) points out the global stability of the time series. This stability is at last highlighted by the devil's staircase in which it is reflected by the filling of steps attached to rational $\delta_{s,i}^{(N_s)}$ and $\delta_{c,i}^{(N_s)}$ whereas the intermediary steep parts of the curve are unoccupied. This outline is actually observed for the experimental time series when the data are not averaged ($N_s=1$). As the sliding window is increased, the series look locally unstable because more and more bits are transferred from the stable to the unstable set of the binary coding, as a result of the low and smoothly varying scaling exponents. However, the steps of the devil's staircase remain filled, indicating that the series are globally convergent.

V. CONCLUSION

Two methods of detecting correlations and possible determinism in the time series of an electronic oscillator were considered. The embedded time series analysis in Sec. III is compatible wih the existence of a hidden attractor of low dimension. On the other hand, the multifractal-type approach in Sec. IV demonstrates remote correlations in the time sequence.

Nonlinear dynamics provides a variety of approaches that may be useful in the context of such experiments. Recently, the study of synchronized states in driven differential equations led to typical mappings of the circle on itself (Arnol'd-type mappings), which could explain physical effects such as the Josephson effect, modulations in a phase locked loop, and cardiac pacemakers [30].

A similar approach was used to account for the interaction of a high-frequency driving signal and a delay line oscillator undergoing a modulational instability. Steps on a frequency-amplitude characteristic are observed at rational ratios between carrier and envelope frequencies in agreement with the deterministic mapping. A stability range of eight orders of magnitude is obtained thanks to that method [31]. This leaves us confident that a deterministic approach using quasiperiodic states may help to understand the low-frequency noise of an electronic oscillator.

[1] D.W. Allan, IEEE Trans. Ultrason. Ferroelec. Freq. Control **34**, 647 (1987).

[2] M. Planat, G. Marianneau, N. Ratier, and F. Lardet-Vieudrin, Appl. Phys. Lett. **67**, 3206 (1995) ; M. Planat, V. Giordano, G. Marianneau, F. Vernotte, M. Mourey, C. Eckert, and J.A. Miehé, IEEE Trans. Ultrason. Ferroelec. Freq. Control **43**, 326 (1996).

[3] E.N. Lorentz, J. Atmos. Sci. **20**, 130 (1963).

[4] N.H. Packard, J.P. Crutchfield, J.D. Farmer, and R.S. Shaw, Phys. Rev. Lett. **45**, 712 (1980).

[5] R. Mané, in *Detecting Strange Attractors in Turbulence*, edited by D.A. Rand and L.S. Young, Lecture Notes in Mathematics Vol. 898 (Springer, Berlin, 1981), p. 230; F. Takens, *ibid.*, p. 366.

[6] P. Grassberger and I. Procaccia, Physica D **9**, 189 (1983).

[7] P. Grassberger and I. Procaccia, Phys. Rev. A **28**, 2591 (1983).

[8] J.C. Roux, R.H. Simoyi, and H.L. Swinney, Physica D **8**, 257 (1983); A. Brandstäter, H.L. Swinney, Phys. Rev. A **35**, 2207 (1987).

[9] A. Wolf, J.B. Swift, H.L. Swinney, and J.A. Vastano, Physica D **16**, 285 (1985); J. Gao and Z. Zheng, Phys. Rev. E **49**, 3807 (1994).

[10] P.E. Rapp, A.M. Albano, T.I. Schmah, and L.A. Farwell, Phys. Rev. E **47**, 2289 (1993).

[11] A.R. Osborne and A. Provenzale, Physica D **35**, 357 (1989); A. Provenzale, L.A. Smith, R. Vio, and G. Murante, *ibid.* **58**, 31 (1992).

[12] A.R. Osborne and A. Pastorello, Phys. Lett. A **181**, 159 (1993).

[13] W. Liebert, K. Pawelzik, and H.G. Schuster, Europhys. Lett. **14**, 521 (1991).

[14] M.B. Kennel, R. Brown, and H.D.I. Abarbanel, Phys. Rev. A **45**, 3403 (1992).

[15] J. Rutman, Proc. IEEE **66**, 1048 (1978).

[16] B. Cunin, F. Heisel, and J. A. Miehé, Appl. Phys. B **53**, 148 (1991).

[17] C. Eckert, Appl. Opt. **34**, 7680 (1995).

[18] E.O. Schulz-Dubois and I. Rehberg, Appl. Phys. **24**, 323 (1981); B. Cunin, C. Eckert, A. Haessler, F. Heisel, J. A. Miehé, and M. Planat, IEEE Trans. Ultrason. Ferroel. Freq. Control **41**, 275 (1994). Note that in this paper a factor 1/2 is missing on the right-hand side of Eq. (2).

[19] A.M. Fraser and H.L. Swinney, Phys. Rev. A **33**, 1134 (1986); A.M. Fraser, Physica D **34**, 391 (1989); W. Liebert and H.G. Schuster, Phys. Lett. A **142**, 107 (1989). Other references are indicated in [13].

[20] A.M. Albano, J. Muench, C. Schwartz, A.I. Mees, and P.E. Rapp, Phys. Rev. A **38**, 3017 (1988).

[21] J. Theiler, Phys. Rev. A **34**, 2427 (1986).

[22] J. Theiler, J. Opt. Soc. Am. A **7**, 1055 (1990).

[23] C. Eckert and J. A. Miehé, Ann. Télécommun. **53**, 351 (1996).

[24] D. Ruelle, Proc. R. Soc. London Ser. A **427**, 241 (1990).

[25] J.P. Eckmann and D. Ruelle, Physica D **56**, 185 (1992).

[26] L.A. Smith, Phys. Lett. A **133**, 283 (1988).

[27] E.J. Kostelich and J.A. Yorke, Physica D **41**, 183 (1990).

[28] D.R. Fredkin and J.A. Rice, Phys. Rev. E **51**, 2950 (1995).

[29] M.C. Gutzwiller, *Chaos in Classical and Quantum Mechanics* (Springer Verlag, New York, 1990), p. 398.

[30] M. Planat and P. Koch, Fractals **1**, 727 (1993).

[31] M. Planat, F. Lardet-Vieudrin, G. Martin, S. Dos Santos, and G. Marianneau, J. Appl. Phys. **80**, 2509 (1996).